LETTER Communicated by Daniel Tranchina

Spiking Neurons and the First Passage Problem

Lawrence Sirovich
lsirovich@rockefeller.edu
Laboratory of Applied Mathematics, Mount Sinai School of Medicine, New York, NY 10029, U.S.A.

Bruce Knight
knight@mail.rockefeller.edu
Center for Studies in Physics and Biology, Rockefeller University, New York, NY 10065, U.S.A.

We derive a model of a neuron's interspike interval probability density through analysis of the first passage problem. The fit of our expression to retinal ganglion cell laboratory data extracts three physiologically relevant parameters, with which our model yields input-output features that conform to laboratory results. Preliminary analysis suggests that under common circumstances, local circuitry readjusts these parameters with changes in firing rate and so endeavors to faithfully replicate an input signal. Further results suggest that the so-called principle of sloppy workmanship also plays a role in evolution's choice of these parameters.

1 Introduction

The pattern of electrical discharge event times, recorded from a neuron by a microelectrode in a vertebrate's central nevous system, largely depends on three macroscale parameters: local synaptic input current s, in response to signals from other neurons, the transmembrane ohmic rate constant γ, proportional to transmembrane conductance, and the intracellular level of stochastic voltage noise, which may be expressed as a diffusion coefficient. Here we develop an expression for a neuron's interspike-interval probability density distribution in terms of these three variables. Our procedure assigns to the recorded neuron a simplified dynamical model, whose input-output dynamics, in some studied cases, conforms well with laboratory results.

We derive a general class of interspike-interval probability distributions based on the three parameters. The best fit of laboratory data within this class furnishes an estimated input current, membrane constant, and level of stochastic activity for the neuron in question.

We have made a natural extension of this methodology to a neuron driven by a naturalistic time-varying stimulus that responds over a

substantial range of firing rates. The manner in which the parameters are seen to change across rates leads to two tentative observations. First, our measured neuron belongs to a subset of design possibilities distinguished by the property that a population of such neurons has a time-dependent firing rate output that, over a considerable dynamic range, is a faithful copy of their synaptic current input. Second, our neuron's design is robust against substantial construction errors and thus conforms to the so-called principle of sloppy workmanship.

2 Formulation

The five layers of the retina, one of which is the layer of retinal ganglion cells, can process image information in as little as 15 msec (Kaplan & Benardete, 2001; Maunsell et al., 1999). Compared with interspike times, this provides compelling evidence that synaptic dynamics is fast compared to membrane potential encoding, and we consider a model that depends on only the membrane potential. This was also the case in the early studies by Stein (1965) and Wilbur & Rinzel (1982) that modeled encoding neurons by membrane voltage jumps.

The membrane potential, V, can be made dimensionless by the substitution $x = (V - V_r)/(V_t - V_r)$, where V_r and V_t are the dimensional resting and threshold potentials, so that $x \leq 1$, where $x = 0$ is the resting potential and $x = 1$ is the voltage threshold for firing. Thus, we consider a probability density, $\rho(x, t)$, for the membrane potential x at time t. In general, the time course of ρ is determined by a continuity equation,

$$\frac{\partial}{\partial t}\rho(x, t) = -\frac{\partial}{\partial x} J[\rho], \tag{2.1}$$

where J, the probability flux, is a linear functional of ρ that depends on inputs and defines the dynamics of the encoding neuron (Stein, 1965; Wilbur & Rinzel, 1982, 1983; Abbott & van Vreeswijk, 1993; Knight, Manin, & Sirovich, 1996; Knight, 2000; Omurtag, Knight, & Sirovich, 2000; Nykamp & Tranchina, 2000). The distribution of interspike intervals follows from the first passage problem, in which

$$\rho(x, t = 0) = \delta(x) \tag{2.2}$$

and boundary conditions

$$\rho(1, t) = 0 = \rho(-\infty, t), \tag{2.3}$$

where the first is the absorbing boundary condition at the firing threshold. The evolution of the distribution $\rho(x, t)$ over voltage is governed by the form of J in equation 2.1 and by equation 2.3. In instances of interest, its

evolution is dominated by drift toward higher voltage, and back diffusion is slight. This serves as a basis for the convenient assumption that $x \in (-\infty, 1)$, which we adopt.

The structure of equations 2.1 to 2.3 above implies that while the occurrence time of a given spike clearly depends on that of its predecessor, it is independent of all earlier spiking history. Technically we are dealing with a renewal process. Troy and Robson (1992) present data to show that this is a reasonable approximation for retinal ganglion cells.

Following a standard argument, the probability that no spike has occurred and the neuron still lies in the interval $(-\infty, 1)$ at time t is given by

$$\int_{-\infty}^{1} \rho(x, t)\, dx = 1 - P(t), \tag{2.4}$$

and thus $P(t)$ is the probability of escape in the time t. On differentiating this expression with respect to time, from equation 2.1, we can perform the integral and obtain the rate of probability escape,

$$\mathcal{P}(t) = \frac{dP}{dt} = J_o = J[\rho]\big|_{x=1}, \tag{2.5}$$

which is the interspike interval probability distribution. It is immediate from equation 2.2 that

$$\int_{0}^{\infty} \mathcal{P}(t)\, dt = 1. \tag{2.6}$$

The gold standard for describing neuronal firing is the Hodgkin-Huxley system, but the earlier phenomenological leaky-integrate-and fire model

$$\frac{dx}{dt} = -\gamma x + s, \tag{2.7}$$

with firing threshold $x = 1$ and resting state $x = 0$, has proven a trustworthy approximation when the input timescale is large compared to the duration of the action potential (Knight, 1972; Keener & Sneyd, 1998; Dayan & Abbott, 2001; Carrillo & Hoppensteadt, 2010). Equation 2.7 models the activity of the membrane by an RC circuit where γ represents leakage conductance and s is the input current.

The model just defined is a greatly simplified representation of the actual physical mechanisms that underlie the generation of interspike intervals in a real retinal ganglion cell. Nonetheless, neurons respond to one another only through the timing of the spikes that they receive. We will see that this compact model succeeds in describing a retinal ganglion cell's measured interspike interval statistics.

Because of our scaling to dimensionless voltage in equation 2.7, s, like γ, carries the physical dimension of (time)$^{-1}$ or rate. We note that if s is constant and $s < \gamma$, then equation 2.7 has an equilibrium solution

$$x_e = s/\gamma = \widehat{s}\,; \tag{2.8}$$

otherwise equation 2.7, which is explicitly integrable, leads to periodic firing. The dimensionless ratio $\widehat{s}$ plays a natural role in the theoretical analysis below.

A natural dimensionless rescaling of time,

$$\tau = \gamma t, \tag{2.9}$$

brings equation 2.7 to the convenient one-parameter form

$$\frac{dx}{d\tau} = -x + \widehat{s}, \tag{2.10}$$

which, for $\widehat{s} < 1$, gives a voltage $x(\tau)$ that relaxes at unit exponential rate from $x(0) = 0$ to the equilibrium equation 2.8:

$$x(\tau) = \widehat{s}(1 - \exp(-\tau)). \tag{2.11}$$

A model of a neuron with noise is obtained by augmenting the causal current s in equation 2.7 with stochastic fluctuations. This situation may be addressed by considering an ensemble of neurons, and from this the probability density $\rho(x, t)$ over their voltages x, as it evolves in time. For fluctuations that are frequent, small, and brief, several forms of argument (Gardiner, 2009; also see Knight et al., 1996) show that equation 2.7 leads to a diffusion equation for $\rho(x, t)$,

$$\frac{\partial \rho}{\partial t} = \frac{\partial}{\partial x}\left[(\gamma x - s)\rho + D\frac{\partial \rho}{\partial x}\right], \tag{2.12}$$

with initial condition 2.2 and boundary conditions 2.3.

The diffusion coefficient D, which incorporates stochastic effects, here carries the physical dimension of rate. The advective first term of equation 2.12, inherited from equation 2.7, near $x = 0$ indicates flow to the right, while the diffusive term produces a dispersion of the δ-function as it is transported.

Equation 2.12, termed a Fokker-Planck equation, and more particularly the Ornstein-Uhlenbeck equation, was explored by Smoluchowski and Schrödinger early in the twentieth century (Uhlenbeck & Ornstein, 1930; also see Smoluchowski, 1915; Chandrasekhar, 1943; Risken, 1996; Gardiner,

2009; van Kampen, 2007). Schrödinger (1915) eloquently remarks on the analytical intractability of the first passage problem. The potential value of a tractable analytical solution of the first passage problem has led to investigations on exact but largely indirect approaches (Siegert, 1951; Ricciardi, 1977; Sampath & Srinivasan, 1977; Iyengar, 1996), and numerical approaches (Mullowney & Iyengar, 2007; Plesser & Geisel, 1999). In the following, some new features of the first passage problem are investigated, including exact and asymptotic results, which may be of general interest.

3 Transformations

Features of the solution to equation 2.12 become evident when it is recast by simple transformations of variables. In particular, we define

$$\epsilon = D/\gamma \tag{3.1}$$

and apply this and equation 2.9 to equation 2.12 to obtain

$$\frac{\partial \rho}{\partial \tau} = \frac{\partial}{\partial x}\left[(x - \widehat{s})\rho + \epsilon \frac{\partial \rho}{\partial x}\right], \tag{3.2}$$

a two-parameter dimensionless equation. The initial and boundary conditions equations 2.2 and 2.3 remain intact. Solutions of equation 2.12 may be directly constructed from those of equation 3.2.

A further substitution,

$$x = 1 - y, \tag{3.3}$$

puts equation 3.2 onto the half-infinite line $0 \leq y \leq \infty$ with boundary conditions (from equation 2.3)

$$\rho(0, \tau) = 0, \quad \rho(\infty, \tau) = 0 \tag{3.4}$$

and initial condition

$$\rho(y, 0) = \delta(y - 1), \tag{3.5}$$

so that equation 3.2 becomes

$$\frac{\partial \rho}{\partial \tau} = \frac{\partial}{\partial y}\left[(y - (1 - \widehat{s}))\rho + \epsilon \frac{\partial \rho}{\partial y}\right]. \tag{3.6}$$

The substitution

$$y = \sqrt{\epsilon} z \tag{3.7}$$

and definition

$$\beta = (\widehat{s} - 1)/\sqrt{\epsilon} \tag{3.8}$$

reduce equation 3.6 to the one-parameter form,

$$\frac{\partial \rho}{\partial \tau} = \frac{\partial}{\partial z}\left[(z + \beta)\rho + \frac{\partial \rho}{\partial z}\right] = \mathcal{L}\rho, \tag{3.9}$$

with initial condition

$$\rho(z, 0) = \delta(z - z_*); \quad z_* = 1/\sqrt{\epsilon}. \tag{3.10}$$

The boundary conditions continue to be equation 3.4. The signature of β determines whether $\widehat{s} < 1$ or $\widehat{s} > 1$, which, as foreshadowed by the nonstochastic case 2.7, leads to different consequences. An asymptotic treatment given in the appendix brings this dichotomy into sharp focus.

The general treatment leading to equation 2.5 applies to equation 3.9, and it is immediate that the first passage density is given by

$$\mathcal{P}(\tau; \beta, z_*) = \frac{\partial}{\partial z}\rho(z, \tau; \beta, z_*)\big|_{z=0} \tag{3.11}$$

since ρ vanishes at $z = 0$.

Clearly there is an immediate map between the solutions of equation 3.9 and those of equation 3.2.

4 Background Results

The solution of the initial value problem of equation 3.9 with equation 3.10 on the fully infinite line is exactly given by

$$\widehat{\rho}(z, \tau; \beta, z_*) = (2\pi v(\tau))^{-1/2} \exp(-(z + \beta - (z_* + \beta)e^{-\tau})^2)/2v(\tau)), \tag{4.1}$$

where

$$v(\tau) = 1 - \exp(-2\tau). \tag{4.2}$$

This solution, known to Schrödinger (1915), has the form of a time-dependent gaussian with variance $v(\tau)$ and mean

$$\bar{z} = z_* e^{-\tau} - a(\tau), \tag{4.3}$$

where

$$a(\tau) = \beta(1 - e^{-\tau}). \tag{4.4}$$

Here $\bar{z}(\tau)$ is, in our present variables, the exponential relaxation time course obtained by integrating equation 2.7. If we let $\tau \to 0$, then $\widehat{\rho}$ becomes the δ-function of equation 3.10, and when $\tau \to \infty$, we see that $\widehat{\rho}$ approaches the steady state

$$\widehat{\rho}(z, \infty; \beta, z_*) = \frac{1}{\sqrt{2\pi}} e^{-(z+\beta)^2/2}. \tag{4.5}$$

In the special case $\beta = 0$, equation 3.9 becomes

$$\frac{\partial \rho}{\partial \tau} = \frac{\partial}{\partial z}\left[z\rho + \frac{\partial \rho}{\partial z} \right], \tag{4.6}$$

which is symmetric about $z = 0$, so that not only $\widehat{\rho}(z, \tau; 0, z_*)$ but also $\widehat{\rho}(-z, \tau; 0, -z_*) = \widehat{\rho}(z, \tau; 0, -z_*)$ solves equation 4.6 on the full infinite line, and their difference,

$$\rho^o(z, \tau) = \widehat{\rho}(z, \tau; 0, z_*) - \widehat{\rho}(z, \tau; 0, -z_*), \tag{4.7}$$

vanishes at $z = 0$ and thus also is an exact solution of the sought-after half-infinite-line first passage problem.

Continuing with the $\beta = 0$ case, we calculate the exact first passage density from equation 3.11 to be

$$\mathcal{P}(\tau) = \frac{\partial}{\partial z} \rho^o(z, \tau)\big|_{z=0} = \sqrt{\frac{2}{\epsilon\pi}} \frac{e^{-\tau}}{(1 - e^{-2\tau})^{3/2}} \exp\left(- \frac{1}{2\epsilon(e^{2\tau} - 1)} \right). \tag{4.8}$$

The only parametric dependence is on $z_* = \sqrt{\gamma/D} = \sqrt{1/\epsilon}$. If z_* and τ are back-substituted in terms of γ, s, D, and t, the result proves to be equivalent to that noted by Ricciardi (1977), Sampath and Srinivasan (1977), and Iyengar (1996) (see also Bulsara, Elston, Doering, Lowen, & Lindenberg, 1996).

The exact result of equation 4.8, for the special case of $\beta = 0$, serves as a check on our calculation for general β below. Also $\beta = 0$ fits well to the ganglion cell data later shown in Figures 3 and 4.

5 Exact Analysis

While the asymptotic first passage densities developed in the appendix may be used to analyze data, with only little additional labor, precise numerical densities may be obtained and offer the preferred analysis method.

To implement this, we introduce the Laplace transform,

$$\tilde{\rho}(q, \tau) = \int_0^\infty e^{-qz} \rho(z, \tau)\, dz, \tag{5.1}$$

which, applied to equation 3.9, yields

$$\frac{\partial \tilde{\rho}}{\partial \tau} = -q \frac{\partial \tilde{\rho}}{\partial q} + (\beta q + q^2)\tilde{\rho} - \mathcal{P}(\tau) \tag{5.2}$$

with the initial condition, from equation 3.10, given by

$$\tilde{\rho}(\tau = 0) = \int_0^\infty e^{-qz} \delta(z - z_*)\, dz = e^{-qz_*}. \tag{5.3}$$

The first-order partial differential equation, 5.2, with initial condition 5.3, may be solved by the method of characteristics to give

$$\begin{aligned} \tilde{\rho}(q, \tau) = &\exp[-z_* q e^{-\tau} + \beta q (1 - e^{-\tau}) + q^2 (1 - e^{-2\tau})/2] \\ &- \int_0^\tau \exp[\beta q (1 - e^{-(\tau - \tau')}) + q^2 (1 - e^{-2(\tau - \tau')})/2]\, \mathcal{P}(\tau') d\tau', \end{aligned} \tag{5.4}$$

which is in terms of the still unknown first passage density $\mathcal{P}(\tau; \beta, z_*)$. The inverse transform of equation 5.4 may also be executed in explicit form, which yields the relationship between ρ and $\mathcal{P}$,

$$\rho(z, \tau) = \frac{e^{-(z - z_* e^{-\tau} + a(\tau))^2 / 2v(\tau)}}{\sqrt{2\pi v(\tau)}} - \int_0^\tau d\tau' \mathcal{P}(\tau') \frac{e^{-(z + a(\tau - \tau'))^2 / 2v(\tau - \tau')}}{\sqrt{2\pi v(\tau - \tau')}}, \tag{5.5}$$

where $v(\tau)$ and $a(\tau)$ are defined by equations 4.2 and 4.4, respectively.

In particular, equation 5.5 holds at $z = 0$, where ρ vanishes and the equation becomes a relation involving $\mathcal{P}$ alone, given by

$$\frac{e^{-(z_* e^{-\tau} - a(\tau))^2/2v(\tau)}}{\sqrt{2\pi v(\tau)}} = \int_0^\tau d\tau' \mathcal{P}(\tau') \frac{e^{-a(\tau-\tau')^2/2v(\tau-\tau')}}{\sqrt{2\pi v(\tau-\tau')}}, \tag{5.6}$$

a Volterra integral equation for the first passage density $\mathcal{P}(\tau; \beta, z_*)$. It may easily be discretized as a standard set of inhomogeneous linear equations and numerically solved in roughly 1 second on a desktop, and in a short time, a high-resolution catalog of such distributions may be generated. With the substitution $z_* = 1/\sqrt{\epsilon}$, we have done this for ϵ and β values that cover what appears to be a reasonable range for retinal ganglion cells.

6 Application to Data

A further time scaling is needed to match theoretical and experimental data. Experimental interspike-interval records lead to an estimate of the experimental interpulse density $\mathcal{P}_{\exp}(t)$, which in turn yields the mean interval $\langle t \rangle$. For a range of inputs, $\langle t \rangle$ may cover a range of values, and for parameter determination, it is convenient to put such distributions on a common footing by rescaling time,

$$\hat{t} = t/\langle t \rangle, \tag{6.1}$$

so that the corresponding density scaling becomes

$$\hat{\mathcal{P}}_{\exp}(\hat{t}) = \langle t \rangle \mathcal{P}_{\exp}(\langle t \rangle \hat{t}). \tag{6.2}$$

For any $\hat{\mathcal{P}}_{\exp}(\hat{t})$, the mean value of $\hat{t}$ is unity, so we can now compare the shapes of distributions free from the confounding feature of variable duration. The theoretical distributions are likewise renormalized by

$$\langle \tau \rangle = \int_0^\infty \tau \mathcal{P}_{th}(\tau)\, d\tau \tag{6.3}$$

and

$$\hat{\mathcal{P}}_{th}(\hat{t}) = \langle \tau \rangle \mathcal{P}_{th}(\langle \tau \rangle \hat{t}), \tag{6.4}$$

so that experimental and theoretical distributions are now on a common footing.

Out of the array of theoretical distributions in the catalog, we seek the best match to data (e.g., by a least squares method). Once the parameters

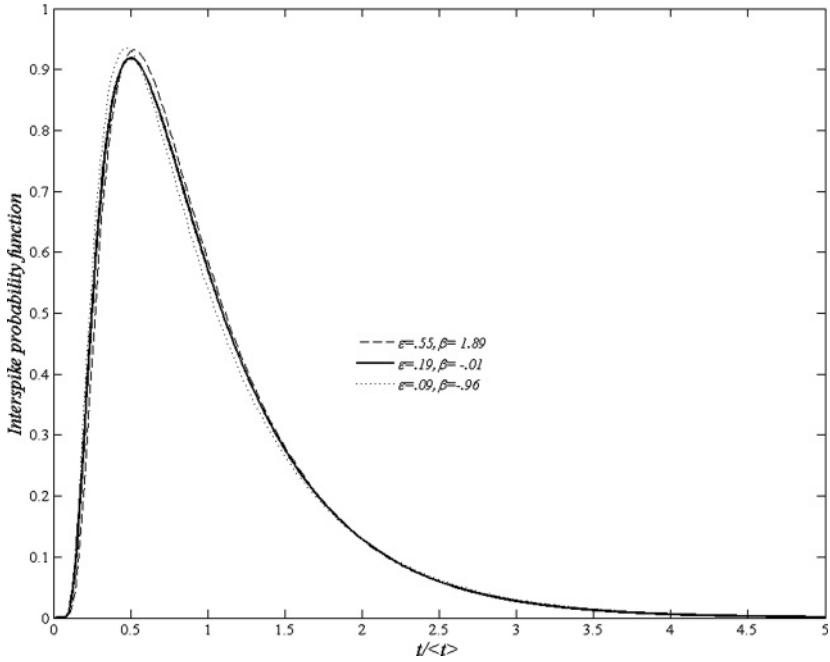

Figure 1: Three plots of $\widehat{P}_{th}(\hat{t};\epsilon,\beta)$ for the indicated parameter values.

ϵ and β are determined on the basis of best match, we observe that since $\tau = \gamma t$, the effective rate constant γ is determined by

$$\gamma = \langle\tau\rangle/\langle t\rangle. \tag{6.5}$$

From this, the diffusion coefficient is given by

$$D = \gamma\epsilon \tag{6.6}$$

and the scaled membrane current by

$$s = \gamma(1+\beta\sqrt{\epsilon}), \tag{6.7}$$

thus fixing the three macroscales of the experimental data.

Examination of our catalog of uniformly scaled first passage distributions, above, shows that great care must be exercised in the procedure for deriving a least-mean-square fitting. In Figure 1 we show three calculated $\widehat{P}_{th}(\hat{t};\epsilon,\beta)$ distributions for three quite different choices of (ϵ,β) pairs.

Each of these three curves is quite a good match, by eye, to a particular experimental first passage density obtained from a retinal ganglion cell. The three curves also, by eye, appear to be close approximations of one another, and if weight is given to maximum height, then the two curves with parameters that lie at opposite extremes are more similar to each other than to the curve whose parameters lie between theirs. The figure suggests that even an optimal fitting procedure might at best present alternatives among which we must choose by criteria other than curve shape.

A procedure for fitting experimental first passage data to a best-matched member in a catalog of first passage density functions should satisfy several basic criteria (1) it should be insensitive to improbable experimental outliers, (2) should use all the information in the experimental data, and (3) It should not be biased toward any particular members or regions of the catalog.

A linear least-mean-square fitting procedure is natural. Criterion 1 guides us to choose, as a starting point, not the density function but rather its cumulative probability:

$$C(\hat{t}) = \int_0^{\hat{t}} \mathcal{P}(\hat{t}')\, d\hat{t}'. \tag{6.8}$$

This probability function has the range $0 \leq C \leq 1$. In experimental data, improbably large outlier values of $\hat{t}$, regardless of their size, yield a corresponding C value near unity.

If probability is used as an independent variable, say, c, then as a dependent variable, $\hat{t}$ is related to it through the inverse function

$$\hat{t} = C^{-1}(c). \tag{6.9}$$

In particular for a theoretical first passage distribution with parameters ϵ, β, we may write

$$\hat{t} = C_{\epsilon\beta}^{-1}(c). \tag{6.10}$$

We use equation 6.9 in the fitting of laboratory data to theory. If our data constitute N interpulse intervals of which the jth is $\hat{t}_j$, then a data-based first passage density

$$\mathcal{P}_d(\hat{t}) = \frac{1}{N} \sum_{j=1}^{N} \delta(\hat{t} - \hat{t}_j) \tag{6.11}$$

yields all estimates, such as moments, from those data exactly. As in equation 6.8, equation 6.11 yields the cumulative probability

$$C_d(\hat{t}) = \frac{1}{N}\sum_{j=1}^{N}\int_0^{\hat{t}} d\hat{t}'\delta(\hat{t}' - \hat{t}_j). \tag{6.12}$$

In form, $C_d(\hat{t})$ is a set of N steps, each rising by an increment of $(1/N)$ at a time $\hat{t}_j$. Its inverse function,

$$\hat{t} = C_d^{-1}(c), \tag{6.13}$$

in form is thus a set of uniformly spaced steps, the nth of which steps up at

$$c = c_n = n/N \tag{6.14}$$

and rises at c_n to an accumulated height,

$$\hat{t} = C_d^{-1}(n/N) = \hat{t}_n. \tag{6.15}$$

Arranged in this order, according to increasing size, the $\hat{t}_n$ are the sample's order statistics, widely exploited in the statistical literature (David & Nagaraja, 2003).

If the data make a large N available, then equation 6.12 produces a $C_d(\hat{t})$, which well approximates a smoothly rising curve that rises from zero to unity.

Together, equations 6.10 and 6.15 would yield a least-mean-squared-difference choice procedure in the form of a discrete sum over N terms. However, the top terms of the sum, near and including $\hat{t}_N$, would be (as $\hat{t}$ ranges to infinity) untrustworthy outliers, not conforming to our criterion 1 above. We have gone a step further and have corrected this in a way patterned on the Kolmogorov-Smirnov statistical test (Lupton, 1993) for whether a set of data points was drawn from a given theoretical distribution. However, our test has been refined to utilize all the experimental information (which the Kolmogorov-Smirnov test does not) and so conforms to our criterion 2 above.

We exploit the feature that made our challenge difficult: that all our scaled densities are rather similar in shape. The mean of these densities,

$$\overline{\mathcal{P}}(\hat{t}) = \frac{1}{N(\epsilon,\beta)}\sum_{\epsilon,\beta}\widehat{\mathcal{P}}(\hat{t};\epsilon,\beta), \tag{6.16}$$

does not drastically depart in shape from any member in its sum; it is likewise normalized, and, following equation 6.8, it has a cumulative probability

$$\overline{C}(\hat{t}) = \int_0^{\hat{t}} \overline{\mathcal{P}}(\hat{t}')\, d\hat{t}', \tag{6.17}$$

which ranges up to

$$\overline{C}(+\infty) = 1. \tag{6.18}$$

This transformation of the experimental $\hat{t}_j$ data by equation 6.17 satisfies criteria 1 and 2 above.

Put together equations 6.17, 6.10, and 6.15, and the residual for least-squares optimization is

$$R^2(\{\hat{t}_j\}; \epsilon, \beta) = \frac{1}{N} \sum_{j=1}^{N} [\overline{C}(C_{\epsilon\beta}^{-1}(j/N)) - \overline{C}(C_d^{-1}(j/N))]^2. \tag{6.19}$$

We believe that equation 6.19 meets the challenge of Figure 1 nearly as well as possible, though we believe an expression that does slightly better and is slightly simpler might be advanced.

7 Synthetic Data

To explore these and related issues that arise in dealing with laboratory spike data, we apply our methodology to data generated artificially, over which we have a degree of control. Briefly stated, we randomly draw interspike intervals from a known $\mathcal{P}_{th}(\tau; \epsilon, \beta)$ and apply our matching procedure to these data. Specifically, random values are drawn from the uniform distribution over $(0, 1)$ and inserted in equation 6.10 to obtain a sample of scaled spike times $\hat{t}$. We may then treat these spike times as order statistics data, insert them in equation 6.19 for each pair (ϵ, β) in our catalog, and choose the smallest residual R to see how nearly our procedure recovers the (ϵ, β) parameter values that we put in.

In correspondence with experimental data examined in section 8, we choose

$$(\epsilon^o, \beta^o) = (.19, -.01), \tag{7.1}$$

the parameter values of the middle curve in Figure 1. We assemble 100 synthetic sets, each with 1100 interspike intervals. The resulting (ϵ, β) pairs are shown in Figure 2. As anticipated from Figure 1, many of our random

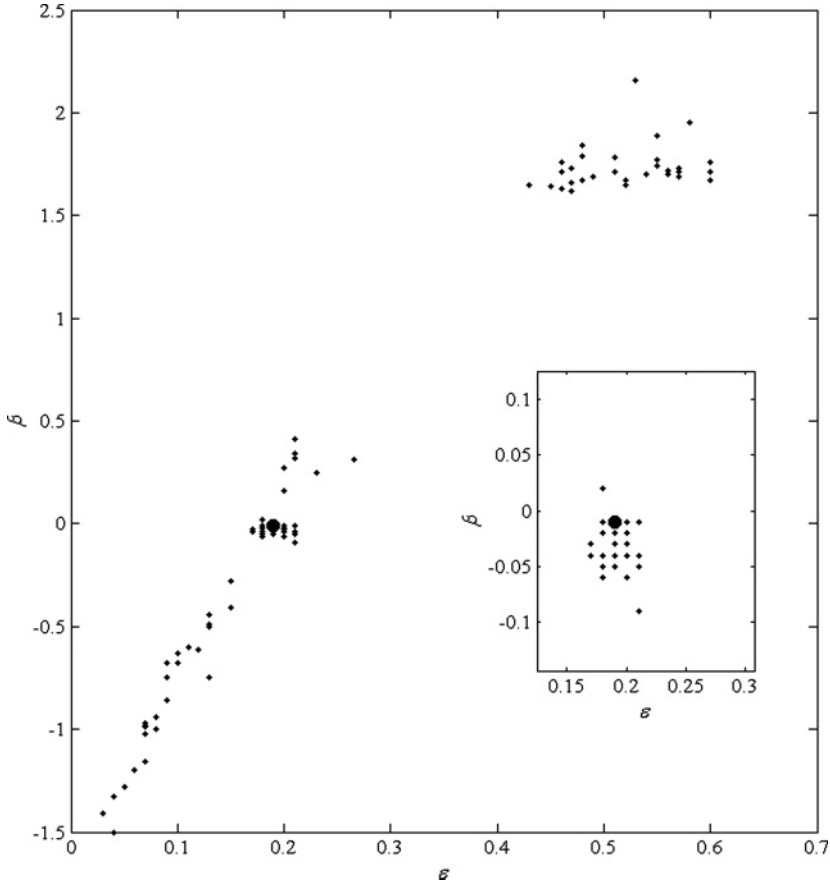

Figure 2: Plot of the 100 (β, ϵ) solutions described in the text. Inset: Blow-up of cluster in neighborhood of equation 7.1.

drawings are better fit by distributions that have a slightly different shape but fairly different parameter values. We first focus on the region of the dark circle, which contains the input parameter values of equation 7.1. The exact parameter values are recovered for 13 of our 100 randomly drawn interspike-interval sets. The inset to the figure expands the vertical scale of that region, where $\epsilon = .19$ occurs 17 times and $\beta = -.01$ occurs 16 times, which makes each of these correct values the modal value for the 100 points. With regard to a standard of accuracy reasonable for interpreting biology, all 33 members of the tight cluster within the inset are sufficiently accurate recoveries of the input parameters.

Equation 6.19 defines a Euclidean distance between members of the function space of first passage densities. The (ϵ, β) parameterization of

the densities $\widehat{P}(\hat{t}; \epsilon, \beta)$ defines a two-dimensional surface in that Euclidean space. Both the variation of distributions in Figure 1 and Figure 2's separation of nearby points, in Euclidean space, into separated subsets on the two-dimensional (ϵ, β) surface, suggest that the (ϵ, β) surface is folded back on itself so that parametrically distinct two-dimensional patches are nearby in distance. A range of parameter values consequently yields very similar interspike distributions.

8 Application to Experimental Data

Next we apply the same methodology to a data set selected from a very large database accumulated in our laboratory (Casti et al., 2011; Knight, 2008). The neurons were retinal ganglion cells recorded in anesthetized cats, which were responding to a time-varying naturalistic stimulus (van Hateren, 1997; Reinagel & Reid, 2000). The spike times in response to 128 repetitions of this stimulus were recorded. The means for reducing the resulting data, to a form useful with the methods above, merits brief discussion.

If the spike times in N statistically independent repeat trials (where $N = 128$ in our case) are merged to a single time record then in this merged record, every spike time is preceded, and also is followed, by roughly N uncorrelated spike times. Consequently, if N is large, the merged record may be conveniently viewed as a sample of an inhomogeneous Poisson point process. An inhomogeneous Poisson process is fully characterized by a rate function over time, which we may call

$$Nr(t). \tag{8.1}$$

Here the factor N is included to put $r(t)$ on a single-trial basis. With large N, the merged sample is able to yield a good estimate of $r(t)$, essentially by maximum likelihood estimation. With $r(t)$ on hand, we can go back to our 128 individual trials and to each spike time record attach a value of $r(t)$ and also a value of $\dot{r}(t)$, its time derivative. Each single-trial interspike interval from the 128 trials therefore can be ordered by the size of r or by how rapidly $r(t)$ is changing.

The function $r(t)$ changes smoothly with t and is of bounded variation. These two properties together endow it with the feature that it spends much of its time near its local extrema, where $r(t)$ is changing only gradually. From our actual ordered list of interspike intervals, we observe that for the middle one-third, $r(t)$ is changing slowly enough to be considered steady. In that smaller set, the values of $r(t)$ smoothly span an order of magnitude. We have reordered that set in the order of rising $r(t)$ and have divided it into seven numerically equal subsets. Each subset well approximates a set of interspike intervals obtained in steady conditions at a particular mean firing rate and is appropriate for the analysis that we applied above to the

Table 1: Parameter Determinations for the Seven Quasi-Steady Firing Rates.

Line	Rate (Hz)	ϵ	β	s/γ	γ	Corrected γ
1	7.2387	0.19	−0.68	0.7036	0.0227	0.0146
2	19.845	0.2	−0.06	0.9732	0.0313	0.0309
3	32.18	0.21	−0.01	0.9954	0.0487	0.0501
4	45.7041	0.19	−0.01	0.9956	0.0757	0.0757
5	59.2168	0.19	−0.01	0.9956	0.0978	0.0978
6	75.1841	0.45	1.58	2.0599	0.0437	0.1196
7	104.8552	0.34	1.35	1.7872	0.0663	0.1499

pseudodata. Over the seven sets, mean firing rate ranges from 7.2387 Hz to 104.8552 Hz. The results of the analysis are given in Table 1. Each of the seven cases contained (close to) 1100 interspike intervals, which accounts for this choice in dealing with the pseudodata in the previous section.

From Table 1 we observe that the mode for ϵ is .19, and for β it is $-.01$, explaining the values chosen in the previous section. Inspection of the table shows several large parameter jumps of the sort we encountered in the previous section. If we compare the scaled density $\widehat{\mathcal{P}}(\hat{t}; \epsilon, \beta)$ for row 6, on the basis of $(\beta, \epsilon) = (1.58, .45)$, with that of row 5 with $(\beta^o, \epsilon^o) = (-.01, .19)$, we obtain a near identity of the two, in the same spirit as Figure 1. The value of γ in the former case is at odds with the natural continuity that is expected. The last column calculates γ on the premise that $\widehat{\mathcal{P}}(\hat{t}; \beta^o, \epsilon^o)$ is the correct fit. We next consider the issue of parameter fitting from another perspective.

8.1 Finite Jump Model. We concluded the paragraph that introduced Figure 1, in section 6, with the suggestion that parameter choice might require data beyond those that determine curve shape. To do that, we now generalize to a finite-jump model for which there exist further data. As we pointed out in section 2, the dynamics of retinal ganglion cell is a consequence of fast synaptic dynamics and is formulated in terms of the membrane voltage alone. Within this set of models is one that includes the possibility of finite jumps in the membrane voltage (Stein, 1965; Wilbur & Rinzel, 1982; Omurtag et al., 2000; Sirovich, Knight, & Omurtag, 2000.)

In the notation of equation 2.1, this model takes on the form

$$J = -\gamma x - \frac{s}{h}\{\rho(x-h) - \rho(x)\} - \kappa \frac{\partial \rho}{\partial x}, \tag{8.2}$$

where the first term is the usual leakage, and the second is the flux due to finite membrane voltage jumps, h, that arrive at a rate s/h, where s is the current. Also included here is a diffusion term with diffusivity κ to account for possible background noise not necessarily associated with the

synaptic arrival rate. If equation 8.2 is substituted in equation 2.1 and the transformation 2.9 is applied, we obtain

$$\frac{\partial}{\partial \tau}\rho = \frac{\partial}{\partial x}(x\rho) + \frac{\widehat{s}}{h}\{\rho(x-h) - \rho(x)\} + \frac{\kappa}{\gamma}\frac{\partial^2 \rho}{\partial x^2}. \tag{8.3}$$

Note that $1/h$ may be regarded as the approximate number of jumps needed to reach the spiking threshold. Freed (2005) has carefully analyzed quantal arrivals for retinal ganglion cells in cat, and according to his study, an average of 10 jumps is needed for spike firing; this suggests that $h \approx .1$. By customary standards, this lies at the borderline of h being small.

The Ornstein-Uhlenbeck equation may be derived from equation 8.3 under the hypothesis that h is small. A simple expansion of $\rho(x-h)$ through order h^2 yields

$$\frac{\partial \rho}{\partial \tau} = \frac{\partial}{\partial x}\left\{(x-\widehat{s})\rho + \left(\frac{\widehat{s}h}{2} + \frac{\kappa}{\gamma}\right)\frac{\partial \rho}{\partial x}\right\}, \tag{8.4}$$

which is of the form 3.2.

It therefore follows that ϵ, which by equation 3.2 is the coefficient of $\partial\rho/\partial x$ in the braces, may be written (using equation 2.8) as

$$\epsilon = \widehat{s}\left(\frac{h}{2} + \frac{\kappa}{s}\right). \tag{8.5}$$

For lines 2 to 5 of Table 1, it may be reasonably supposed that $\widehat{s} \approx 1$ and $\epsilon \approx .19$. If these and Freed's estimate of h are substituted into equation 8.5, we obtain

$$\kappa = .14s. \tag{8.6}$$

If this is back-substituted into equation 8.5, we obtain

$$\epsilon = \widehat{s}\left(\frac{h}{2} + .14\right). \tag{8.7}$$

With this result, which relates h to ϵ, we may now go back to the suspect lines 1, 6, and 7, from which the values of ϵ give h values of .26, .16, and 1, an overall lack of agreement with Freed's measurements

From another perspective, if we regard the (ϵ, β) values of Table 1 on the plot of Figure 2, rows 1, 6, and 7 as just calculated correspond to outlier branches, while rows 2 to 5 are in the close neighborhood of the correct point. This suggests that we adjust lines 1, 6, and 7 in accordance with

$\mathcal{P}(\hat{t}; 0, -.01, .19)$. If this is done, we get the corrected values of γ shown in the last column of the table.

9 A Model Ganglion Cell

Inspection of Table 1 suggests that for lines 2 to 5, $\beta \approx 0$ would be a reasonable approximation. In addition, the discussion in the previous section strongly suggests that lines 1, 6 and 7 represent determinations from an unsuitable branch, in the sense of Figure 2, and might reasonably be fit by $\beta = 0$. This in turn suggests the theoretically exact case of section 4: that $\beta = 0$ is respected throughout the time variation.

Within this framework, the fit of data to our model in Table 1 suggests that the membrane "constant" varies in time

$$\gamma = \gamma(t), \tag{9.1}$$

in such a manner that

$$\hat{s} = s(t)/\gamma(t) = 1. \tag{9.2}$$

Further, this suggests that its neuronal output faithfully follows the stimulus (see Knight, 1972, for an early discussion of such issues). Thus, it appears that we might reasonably collapse the whole time-dependent situation to a compact approximate model by substituting equation 9.2 into equation 3.2, assuming ϵ is constant as indicated by lines 2 to 5 of Table 1:

$$\frac{\partial}{\partial \tau}\rho = \frac{\partial}{\partial x}\left[(x-1)\rho + \epsilon \frac{\partial \rho}{\partial x}\right]; \tag{9.3}$$

and, as equation 9.2 gives $\gamma(t) = s(t)$, equation 2.9 generalizes in a natural way to

$$\tau = \int^t s(t')\, dt'. \tag{9.4}$$

We refer to this as the faithful copy model with $\beta = 0$. Under conditions 9.1 and 9.2, the first passage density is explicitly given by equation 4.8, a one-parameter family in ϵ.

As a test of whether this has some generality, we consider the classic results of Troy and Robson (1992), which they kindly furnished to us in histogram form. The fit of the faithful copy model interspike interval density, equation 9.3, to two of their histograms is shown in Figure 3.

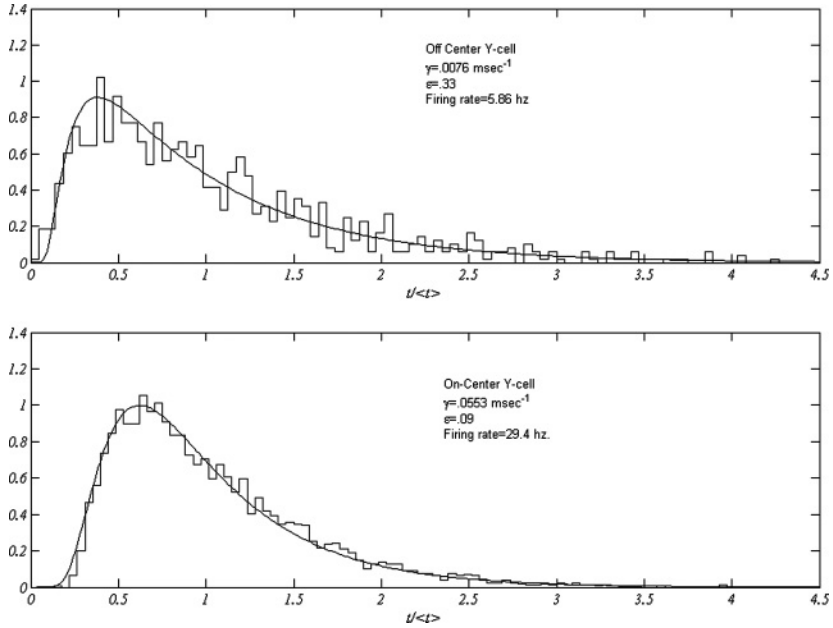

Figure 3: Comparison of $\beta = 0$ probability densities with the results of Troy and Robson (1992).

10 Discussion

We have presented a method for extracting, from neuron spike train data sets, three parameters that characterize a simplified neuron model. These parameters characterize the neuron's momentary synaptic input current, its ohemic rate constant, and its level of intracellular noise. The values of these parameters are determined from the shape of a interspike-interval histogram by means of a three-parameter fit. Study of the model itself, and also results of its application to laboratory data, leads to two nonobvious findings that may be of some physiological interest.

The first finding is that actual neurons measured in the laboratory have chosen a region of physiological parameter space where the firing statistics are remarkably insensitive to the choice of these parameters. In Figure 1, where a parameter has been removed by normalization in terms of firing rate, we see that substantial changes in the two remaining parameters have a very slight effect on the interspike-interval histogram. In Figure 2, we show the converse: from a theoretical infinite-sample limit histogram with parameters chosen to fit a real cell, we have made a 100-member set of 1100-draw Monte Carlo samples, and we have reevaluated our parameters for each of the 100 resulting histograms. As the widely dispersed points in

Figure 2 testify, a wide variety of parameter pairs emerges, from those very similar histograms.

Interacting neurons influence one another only through the occurrence times of their spikes. Consequently our observation above leads us to suspect that at least in this application, nature has chosen an operating point where sketchy construction information, leading to a dispersal of parameters among the resulting neuron population, will not noticeably degrade the performance of the network.

In observing this, we follow the early suggestion of Huggins and Licklider (1951) (expanded by Ratliff, 1965) who enunciate the principle of sloppy workmanship, which suggests that nervous tissue was created by an inventor brilliant enough to produce a blueprint that accounted for implementation by a sloppy workman. The suggestion was that there cannot be sufficient room in the genome to furnish detailed design for the entire nervous system. What we note here resembles the observation of Marder and colleagues (Prinz, Bucher, & Marder, 2004; Marder & Goaillard, 2006) that "disparate parameterizations" can lead to "virtually indistinguishable activity." A similar observation appears in Sarkar and Sobie (2010) for Hodgkin-Huxley–like spiking activity. Discussion in these references suggests that use of this principle may be advantageous for survival.

The second potentially interesting nonobvious finding comes from the time-dependent data. Here we find that for our simplified model, two parameters with the physical dimension of rate ($(time)^{-1}$), namely, membrane conductivity and diffusion coefficient, in fact are not constants but rather change with a scaling close to that of the cell's rate of firing. This led us to propose the very simple time-dependent model presented in equations 9.3 and 9.4, which in Figure 3 gave a good time-independent fit to two of Troy and Robson's cells. In Figure 4, we show that this model also fits reasonably well to the data of our cell discussed above. Conformance to the model would demand that in this format, the cell produce the same universal histogram for all of its different levels of firing rate, and indeed the several laboratory histograms superimpose fairly well. However, the theoretical histogram, when converted back to laboratory time at the various firing rates, gives the well-dispersed family of histograms shown in Figure 5. These naturally fit well to the individual data histograms of Figure 4 when those are similarly recast in laboratory time. For the model, these changes with firing rate in Figure 5 follow naturally from the firing rate dependence of leakage rate and of diffusion.

The wide range of values for the membrane constant that has been noted and questioned in the literature (Fohlmeister & Miller, 1997; Freed, 2005) may be due to the tracking feature of γ that appears in our analysis.

The simple model of equations 9.3 and 9.4 is an example of a broad class of possible neuron designs that might carry high survival value. Equation 9.3, which has a current sink at $x = 1$ but no current source, is addressed to the first passage problem. Adding a current source, equal to

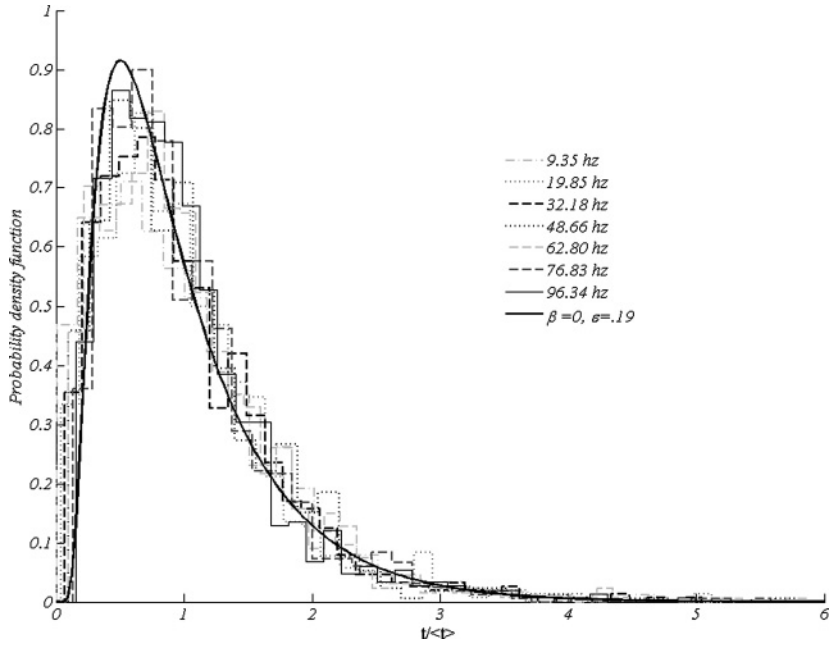

Figure 4: Comparison of the seven cases described in Table 1 with the probability density function $\mathcal{P}(\hat{t} : 0, .19)$.

the sink, at $x = 0$, gives us the full Fokker-Planck equation for the long-time evolution of the neuron ensemble. There is no explicit time dependence in the modified equation 9.3, and it is easily shown that its solution evolves to a steady state that subsequently gives a firing rate, in the variable τ, which is constant (Sirovich et al., 2000). The deterministic neuron (2.10) does not fire in finite time under condition (9.2) but in the presence of noise it does and the firing rate is

$$J_o = s\kappa(\epsilon), \tag{10.1}$$

where the coefficient $\kappa(\epsilon)$ may be explicitly calculated (Sirovich et al., 2000). Thus it may be said that noise takes the membrane potential above the firing threshold, and high current amplifies the process.

Equation 9.4 now tells us that in laboratory time, t, the neuron's firing rate, is proportional to the synaptic input current $s(t)$. That is, the population's time-dependent momentary firing rate is a faithful copy of its synaptic input current. The input-output relation of a neuron population, which has the faithful copy property, thus manages to avoid the typical input-amplitude-dependent strong nonlinearities in output that commonly arise in models of neuron populations based on broadly Hodgkin-Huxley-type neurons. The critical feature of a faithful-copy neuron is that following

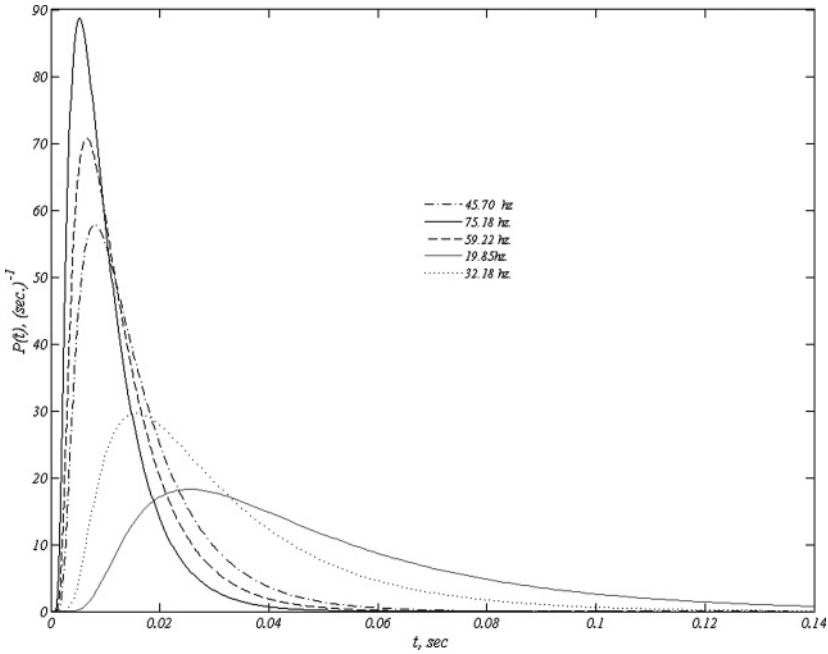

Figure 5: Probability density functions for the middle five cases in dimensional terms.

a change in synaptic input (perhaps an abrupt large change), the population's density distribution over its state-space does not need to seek a different new equilibrium. The fulfillment of the requirements for achieving this is easily understood in equations 9.3 and 9.4. The same way of fulfilling the requirements generalizes naturally to more elaborate realistic neuron models.

As a summary statement the present investigation suggests that *noisiness* and *sloppiness* are essential in the design of nervous tissue.

Appendix: Eigentheory, Limits, and Asymptotics

The Ornstein-Uhlenbeck eigentheory, which follows from equations 3.9 and 3.4, is characterized by

$$\begin{aligned} \mathcal{L}\phi_k &= \frac{\partial}{\partial z}\left[(z+\beta)\phi_k + \frac{\partial \phi_k}{\partial z}\right] = \lambda_k \phi_k \\ \phi_k(0) &= \phi_k(\infty) = 0. \end{aligned} \tag{A.1}$$

An immediate result is that

$$\lambda_k = \lambda_k(\beta), \tag{A.2}$$

thus dropping the analysis down to a one-parameter family, since the eigentheory does not depend on the initial data in equation 3.10, the only place z_* occurs. If

$$\delta(z - z_*) = \sum_n a_n(z_n)\phi_n(z), \tag{A.3}$$

then the first passage solution is given by

$$\rho(z, \tau) = \sum_n a_n \phi_n(z) e^{\lambda_n \tau}. \tag{A.4}$$

We observe that for the full infinite line,

$$\omega(\beta) = e^{-(z+\beta)^2/2} \tag{A.5}$$

satisfies $\mathcal{L}$ of equation A.1 with $\lambda = 0$, and vanishes for $z \to \pm\infty$. Then, as may be verified directly,

$$(\lambda_k, \phi_k) = \left(-k, \frac{\partial^k}{\partial z^k}\omega(\beta)\right) = (-k, \omega(\beta)H_k(z + \beta)); \; k = 0, 1, 2, \ldots \tag{A.6}$$

where H_k is the kth Hermite polynomial (Abramowitz & Stegun, 1970).

From equation A.6 it follows that if β_k is the largest finite positive zero of H_k, then

$$\phi_k(z) = \omega(\beta_n)H_k(z + \beta_n) \tag{A.7}$$

is the principal eigenfunction corresponding to $\lambda = -k$ of the semi-infinite problem A.1, as it satisfies that equation and has no zero crossing for z in $\epsilon(0, \infty)$.

The corresponding eigenvalues are negative integers. Their exactly calculated values are shown in Figure 6 as circles that fall on the continuous curve $\lambda(\beta)$, which is easily computed from the matrix discretization of equation A.1. A principal eigenvalue provides an asymptotic estimate of firing rate.

In the special case of $\beta = 0$, it is clear from equation A.6 that the complete set of eigenfunctions is given by the set ϕ_{2k+1}, $k = 0, 1, \ldots$ corresponding to $\lambda_{2k+1} = -(2k + 1)$. (See Risken, 1996; Gardiner, 2009; van Kampen, 2007.)

In terms of the variables (x, τ), we may write the full infinite domain solution, equation 4.1, as

$$\widehat{\rho}(x, \tau; \beta) = \frac{\exp[-(x - \widehat{s}(1 - e^{-\tau}))^2/2\epsilon v(\tau)]}{[2\pi\epsilon v(\tau)]^{1/2}}, \tag{A.8}$$

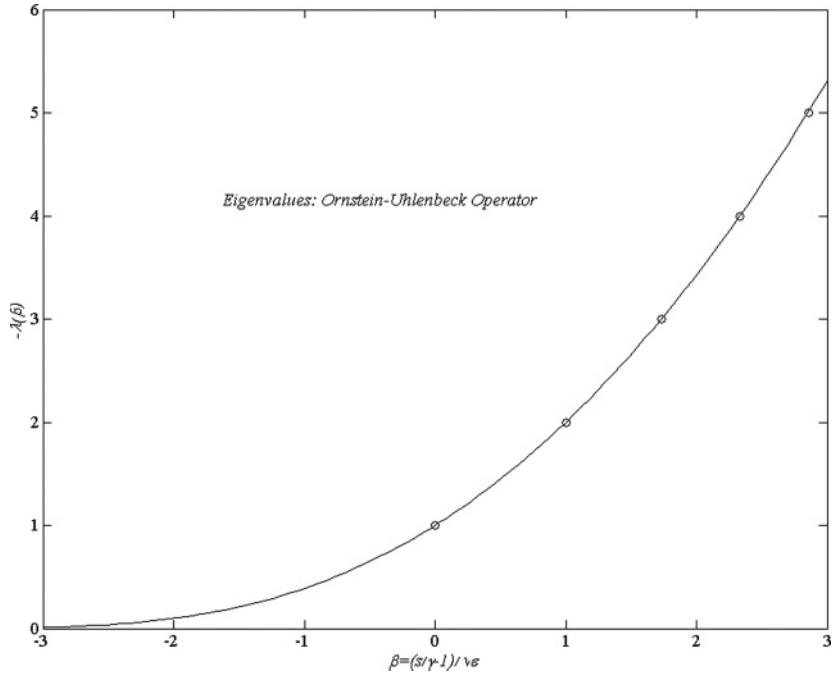

Figure 6: Principal eigenvalue numerically computed from equation A.1. Circles represent the exact considerations.

where $v(\tau)$ is given by equation 4.2. In such terms, the exact first passage solution for $\beta = 0$, equation 4.7, can be put into the suggestive form

$$\rho^o(x, \tau) = \widehat{\rho}(x, \tau; 0)\big(1 - e^{\psi(x,\tau)/\epsilon}\big), \tag{A.9}$$

where

$$\psi(x, \tau) = \frac{-2e^{-\tau}(1 - x)}{(1 - e^{-2\tau})}. \tag{A.10}$$

For $\beta \neq 0$, if we write

$$\rho(x, \tau) = \widehat{\rho}(x, \tau; \beta)g(x, \tau) \tag{A.11}$$

and substitute into equation 3.2, we obtain

$$g_\tau = \frac{\cosh \tau}{\sinh \tau}\left\{ - x + 2\hat{s}\frac{\sinh^2 \tau/2}{\cosh \tau}\right\}g_x + \epsilon g_{xx} = Lg. \tag{A.12}$$

For τ small, this becomes

$$Lg \sim -xg_x/\tau + g_{xx}, \tag{A.13}$$

and in this limit, the solution of equation A.12 is

$$g = 1 - e^{-(1-x)/\epsilon\tau}, \tag{A.14}$$

which is consistent with equation A.9 and therefore equation A.10 in this case is

$$\rho \sim \widehat{\rho}\big(x, \tau; \beta\big)\big(1 - e^{-(1-x)/\epsilon\tau}\big) \tag{A.15}$$

The small time solution for $\widehat{s} \gg 1$ was discussed by Gerstein and Mandelbrot (1964). Equation A.14 exhibits a singular character in the limit $x \to 1$, $\tau \to 0$; however, this is correctly obtained if the first limit is taken as $x \to 1^-$, where 1^- lies to the left of 1.

Next we observe that for τ large, equation A.12 takes the form

$$g_\tau = (-x + \hat{s})g_x + \epsilon g_{xx}, \tag{A.16}$$

which for small ϵ may be treated by boundary layer theory. Approximate solutions to equation A.16 can be conveniently treated in the two regimes noted at the close of section 3.

A.1 Case 1: $\hat{s} \leq 1$. Based on equation 4.8, we might write the asymptotic uniform form of the interspike interval distribution as

$$\mathcal{P} = \widehat{\rho}(1, \tau; \beta)\frac{2Ce^{\lambda\tau}}{(1 - e^{-2C\tau})}, \tag{A.17}$$

where λ is the principal eigenvalue for the given value of β. It is easily seen that this tends to the valid limit for $\tau \downarrow 0$ and $\tau \uparrow \infty$, the basis of considering this form. The constant C is determined by the fact that $\mathcal{P}$ is a pdf normalized to unity. For $\hat{s} = 1$, $C = 1$, and we recover the exact result, equation A.9, in which case, $\lambda = -1$. As a consequence, we can also write

$$\rho \approx \widehat{\rho}(x, \tau; \beta)\left(1 - \exp\left[-\frac{2Ce^{\lambda\tau}(1 - x)}{(1 - e^{-2C\tau})\epsilon}\right]\right), \tag{A.18}$$

which for $\hat{s} = 1$ is exact, A.9.

A.2 Case 2: $\hat{s} > 1$. From the eigentheory of section 5, equation A.4 suggests that for τ large,

$$\rho \sim e^{\lambda\tau}\phi, \tag{A.19}$$

where λ is the principal eigenvalue of $\mathcal{L}$, equation 3.9, and ϕ the principal eigenfunction so that

$$(\lambda - 1)\phi = (\beta + z)\frac{\partial\phi}{\partial z} + \frac{\partial^2\phi}{\partial z^2} \tag{A.20}$$

subject to the boundary conditions

$$\phi(0) = \phi(\infty) = 0. \tag{A.21}$$

On formal grounds, if ϵ is small, then β is large in the present case, and we expect a boundary layer at $z = 0$ since convection is to the left, implying a buildup occurring near the origin. This suggests a boundary layer of $O(1/\beta)$ at $z = 0$. In the neighborhood of the origin, the boundary layer solution is easily obtained as

$$\phi \sim A\big(1 - e^{-\beta z}\big), \tag{A.22}$$

with A to be determined from the outer solution, where z is out of the boundary layer. This is given by

$$\phi \sim (\beta + z)^{\lambda - 1}, \tag{A.23}$$

which, since $\lambda < 0$, vanishes as $z \uparrow \infty$, as required by equation A.21.

We go directly to a form that is uniformly valid over the x-interval. In terms of the original variables, when $\tau \uparrow \infty$, this is given by

$$\rho \sim e^{\lambda\tau}\big(1 - e^{-(\hat{s}-1)(1-x)/\epsilon}\big)(\hat{s} - x)^{\lambda - 1}. \tag{A.24}$$

In this case, the interspike interval distribution function is

$$\mathcal{P}(\tau) \sim -\frac{1}{\epsilon}\frac{\partial}{\partial x}\rho\bigg|_{x=1} = e^{\lambda\tau}(\hat{s} - 1)^{\lambda}, \tag{A.25}$$

whereas from equation A.15 for $\tau \downarrow 0$,

$$\mathcal{P}(\tau) \sim \frac{\exp[-1/4\epsilon\tau]}{\tau^{3/2}\sqrt{4\pi\epsilon}}, \tag{A.26}$$

equations A.25 and A.26 can be combined to give

$$\mathcal{P}(\tau) \approx \frac{2Ce^{\lambda}\tau}{1-e^{-2C\tau}} \cdot \frac{1}{\sqrt{4\pi\epsilon\tau}(e^{1/4\epsilon\tau}-1)+(s-1)^{-\lambda}}, \tag{A.27}$$

where, as earlier, C is determined by requiring that

$$\int_0^{\infty} \mathcal{P}(\tau)\, d\tau = 1. \tag{A.28}$$

Unlike the previous case, we do not recover the exact result for $\widehat{s} = 1$, since β, being large, underlies the asymptotics.

We mention in passing that a straightforward perturbation analysis of the eigentheory of section 5 furnishes a description of $\beta \approx 0$.

Acknowledgments

Support for this work came from NIH/NEI EY16224 and NIH/NIGMS P50 GM071558. We gratefully acknowledge helpful discussions with Udi Kaplan in preparing this manuscript. Thanks to John Troy and John Robson for furnishing us with data from their experiments (Troy & Robson, 1992). We are especially grateful to Alex Casti for sharing his unpublished data (Casti et al., 2011), and to Ellen Paley for her careful help in the preparation of this paper and for her great patience with the many drafts that preceded this one.

References

Abbott, L., & van Vreeswijk, C. (1993). Asynchronous states in networks of pulse-coupled oscillators. *PRE, 48*, 1483–1490.

Abramowitz, M., & Stegun, I. (Eds.) (1970). *Handbook of mathematical functions with formulas, graphs and mathematical tables*. Washington, DC: Department of Commerce, National Bureau of Standards.

Bulsara, A., Elston, T., Doering, C., Lowen, S., & Lindenberg, K. (1996). Cooperative behavior in periodically driven noisy integrate-fire models of neuronal dynamics. *Phys. Rev. E, 53*, 3958–3969.

Carrillo, H., & Hoppensteadt, F. (2010). Unfolding an electronic integrate-and-fire circuit. *Biol. Cybern., 102*, 1–8.

Casti, A., Crumiller, M., Kaplan, E., Knight, B., Shirvalkar, P., & Sirovich, L. (2011). *Quantitative physiology hidden in spiking responses to "naturalistic" stimuli.* Unpublished manuscript.

Chandrasekhar, S. (1943). Stochastic problems in physics and astronomy. *Rev. Mod. Phys., 15*, 1–89.

David, H., & Nagaraja, H. (2003). *Order statistics*. Hoboken, NJ: Wiley-Interscience.

Dayan, P., & Abbott, L. (2001). *Theoretical neuroscience: Computational and mathematical modeling of neural systems*. Cambridge, MA: MIT Press.

Fohlmeister, J., & Miller, R. (1997). Impulse encoding mechanisms of ganglion cells in the tiger salamander retina. *J. Neurophysiol., 78*, 1935–1947.

Freed, M. (2005). Quantal encoding of information in a retinal ganglion cell. *J. Neurophysiol., 94*, 1048–1056.

Gardiner, C. (2009). *Handbook of stochastic methods*. Berlin: Springer-Verlag.

Gerstein, G., & Mandelbrot, B. (1964). Random walk models for the spike activity of a single neuron. *Biophys. J., 4*, 41–68.

Huggins, W., & Lieklider, J. (1951). Place mechanisms of auditory frequency analysis. *J. Acoust. Soc. Am., 23*, 290–299.

Iyengar, S. (1996). Parameter estimation for a diffusion approximation to Stein's model. In R. Cuthbertson, R. Paton, & M. Holcombe (Eds.), *Computation in cellular and molecular biological systems* (pp. 265–277). Singapore: World Scientific.

Kaplan, E., & Benardete, E. (2001). The dynamics of primate retinal ganglion cells. *Progress in Brain Research, 134*, 17–33.

Keener, J., & Sneyd, J. (1998). *Mathematical physiology*. Berlin: Springer-Verlag.

Knight, B. (1972). Dynamics of encoding in a population of neurons. *JGP, 59*, 734–766.

Knight, B. (2000). Dynamics of encoding in neuron populations: Some general mathematical features. *Neural Computation, 12*, 473–518.

Knight, B. (2008). *Some hidden physiology in naturalistic spike rasters: The faithful copy neuron.* Available online at http://dspace1.rockefeller.edu/handle/10209/251.

Knight, B., Manin, D., & Sirovich, L. (1996). Dynamical models of interacting neuron populations. In E. C. Gerf (Ed.), *Symposium on Robotics and Cybernetics: Computational Engineering in Systems Applications.* Lille, France: Cite Scientifique.

Lupton, R. (1993). *Statistics in theory and practice*. Princeton: Princeton University Press.

Marder, E. & Goaillard, J.-M. (2006). Variability, compensation and homeostasis in neuron and network function. *Nature Reviews Neuroscience, 7*, 563–574.

Maunsell, J., Ghose, G., Assad, J., McAdams, C., Christen, E., & Noerager, B. (1999). Visual response latencies of magnocellular and parvocellular LGN neurons in macaque monkeys. *Vis. Neurosci., 16*, 1–14.

Mullowney, P., & Iyengar, S. (2007). Parameter estimation for a leaky integrate-and-fire neuronal model for ISI data. *J. Comput. Neurosci., 24*, 179–194.

Nykamp, D., & Tranchina, D. (2000). A population density approach that facilitates large-scale modeling of neural networks: Analysis and an application to orientation tuning. *J. Comp. Neurosci., 8*, 19–50.

Omurtag, A., Knight, B., & Sirovich, L. (2000). On the simulation of large populations of neurons. *J. Comp. Neurosci., 8*, 51–63.

Plesser, H., & Geisel, T. (1999). Markov analysis of stochastic resonance in a periodically driven integrate-and-fire neuron. *Phys. Rev. E, 59*, 7008–7017.

Prinz, A., Bucher, D., & Marder, E. (2004). Similar network activity from disparate circuit parameters. *Nature Neuroscience, 7*, 1345–1352.

Ratliff, F. (1965). *Mach bands: Quantitative studies on neural networks in the retina*. San Francisco: Holden-Day.

Reinagel, P., & Reid, R. (2000). Temporal coding of visual information in the thalamus. *J. Neurosci., 20*, 5392–5400.

Ricciardi, L. (1977). *Lecture notes in biomathematics: Diffusion processes and related topics in biology*. Berlin: Springer-Verlag.

Risken, H. (1996). *The Fokker-Planck equation: Methods of solution and applications*. Berlin: Springer-Verlag.

Sampath, G., & Srinivasan, S. (1977). *Lecture notes in biomathematics: Stochastic models for spike trains of single neurons*. Berlin: Springer-Verlag.

Sarkar, A., & Sobie, E. (2010). Regression analysis for constraining free parameters in electrophysiological models of cardiac cells. *PloS Comput. Biol., 6*, e1000914.

Schrödinger, E. (1915). Zur theorie der fall- und steigversuche an teilchen mit brownscher bewegung. *Physikalische Zeitschrift, 16*, 289–295.

Siegert, A. (1951). On the first passage time probability problem. *Phys. Rev., 81*, 617–623.

Sirovich, L., Knight, B., & Omurtag, A. (2000). Dynamics of neuronal populations: The equilibrium solution. *SIAM J. Appl. Math., 60*, 2009–2028.

Smoluchowski, M. (1915). Notizuber die berechning der brownschen molkularbewegung bei des ehrenhaft-millikanchen versuchsanordnung. *Physikalische Zeitschrift, 16*, 318–321.

Stein, R. (1965). A theoretical analysis of neuronal variability. *Biophys. J., 5*, 173–194.

Troy, J., & Robson, J. (1992). Steady discharges of X and Y retinal ganglion cells of cat under photopic illuminance. *Visual Neuroscience, 9*, 535–553.

Uhlenbeck, G., & Ornstein, L. (1930). On the theory of Brownian motion. *Phys. Rev., 36*, 823–841.

van Hateren, J. (1997). Processing of natural time series of intensities by the visual system of the blowfly. *Vision Res., 37*, 3407–3416.

van Kampen, N. (2007). *Stochastic processes in physics and chemistry* (3rd ed.). Amsterdam: North-Holland.

Wilbur, W., & Rinzel, J. (1982). An analysis of Stein's model for stochastic neuronal excitation. *Biol. Cybern., 45*, 107–114.

Wilbur, W., & Rinzel, J. (1983). A theoretical basis for large coefficient of variation and bimodality in neuronal interspike interval distributions. *J. Theor. Biol., 105*, 345–368.

Received May 24, 2010; accepted November 6, 2010.